Supporting information

Anti-P2 structured $Na_{0.5}NbO_2$ and Its Negative Strain Effect

Xuefeng Wang, Yurui Gao, Xi Shen, Yejing Li, Qingyu Kong, Sungsik Lee, Zhaoxiang Wang*, Richeng Yu, Yong-Sheng Hu and Liquan Chen

1. Experimental section

All the chemicals were of analytical grade and used as received without further purification. Layered $Na_{0.5}NbO_2$ was synthesized by a solid-state reaction of NbO_2 (Alfa Aesar) and Na (1:1 in mole) at 800 °C for 24 h in an evacuated silica tube. The excess Na would react with the trace O_2 and silica in the sealed silica tube. It is worth noticing that $Na_{0.5}NbO_2$ is highly sensitive to O_2 at high temperature and can be easily oxidized to $NaNbO_3$.

Aberration-corrected scanning transmission electron microscopic (STEM) experiments were performed on a JEOL ARM200F transmission electron microscope equipped with double C_S correctors for the condenser lens and objective lens. Annular bright-field (ABF) and high-angle annular dark-field (HAADF) images were acquired at acceptance angles of 11.5-23.0 and 90-370 mrad, respectively. Prior to STEM measurements, samples from cycled electrodes were dispersed in DEC and transferred on a carbon film coated copper grid. The Raman spectra were recorded on a Renishaw Via-Reflex spectrometer (532 nm radiation) with a resolution of 2 cm^{-1}. All the *ex situ* tests were conducted in vacuum and under the protection of flowing Ar upon sample transfer.

The *in situ* X-ray diffraction (XRD) signals were collected on an X'Pert Pro MPD X-ray diffractometer (D8 Advance with a LynxEye_XEdetector, Bruker) with Cu Kα1 radiation (λ=1.5405 Å) and metal beryllium (Be) as the window of a specially designed electrochemical cell. Polytetrafluoroethylene (PTFE) was used as the binder of the current-collector-free electrode.

Ex situ XAS spectra for the Nb K-edge of $Na_{0.5}NbO_2$ samples were collected at beamline 12BM of Advanced Photon Sources (APS) at Argonne National Laboratory. The monochrometer was detuned to 30% of its original intensity to eliminate the high order harmonics. Energy calibration was conducted using the first inflection point of the spectrum of Nb metal foils as the reference. The XANES and FT-EXAFS spectra were processed using the Athena and Artemis software packages.

The working electrodes were prepared by casting the slurry of $Na_{0.5}NbO_2$ or its mixed compounds with MoS_2, $Na_2Ti_3O_7$ and TiO_2, multiwall carbon nano-tube (XF Nano; internal radius 10~20 nm and 10~30 μm long) and sodium alginate (NaAlg) in de-ionized water at a weight ratio of 80:10:10 on a clean Cu current collector. In an Ar-filled glove box, button-type test cells were assembled with Na foil as the counter electrode, glass fiber as the separator, and 1 mol L^{-1} $NaClO_4$ dissolved in a mixture of ethylene carbonate (EC) and diethyl carbonate (DEC) (4:6 in volume) as the electrolyte.

The electrochemical Na-ion intercalation into $Na_{0.5}NbO_2$ and the performance evaluation of $Na_{0.5}NbO_2$ were carried out on a Land BT2000 battery tester (Wuhan, China) at room temperature. The electrode sheets for *ex situ* characterization were obtained by rinsing the cycled electrode sheets with DMC, drying them in a vacuum mini-chamber of the glove-box, and finally transferring into the vacuum chamber of the instrument or tested in an air-tight container.

Computational section

Spin-polarized calculations are performed within the framework of density functional theory (DFT), [1, 2] carried out in the Vienna Ab-initio Simulation Package (VASP) code. [3] The pseudopotentials are established by the projector-augmented wave (PAW) [4] method and the Perdew-Burke-Ernzerh (PBE) [5] of exchange-correlation function. The 2p and 3s states of Na were treated as valence states with Na_pv ($2p^6$ $3s^1$) pseudopotential. As for Nb, the 4s, 5s and 4d states were treated as valence states using Nb_pv ($4p^6$ $5s^1$ $4d^4$) pseudopotential. And for O, the O ($2s^2$ $2p^4$) pseudopotential was adopted. The cutoff energy for the plane-wave basis is 520 eV. The energies were converged within 10^{-5} eV. All atoms in $Na_{0.5}NbO_2$ are relaxed within a 2×2×1 super-cell based on the primitive cell of $NaNbO_2$ until Hellmann–Feynman force convergence is achieved at 0.01 eV $Å^{-1}$ with a 4×4×2 Γ-centered k-mesh. As for the calculations of static charge and density of states (DOS) of electrons, a denser Γ-centered k-mesh of 7×7×4 is adopted. The spacing of the Γ-centered k-meshes for optimizing the structures with NbO_6 octahedrons (O3, O2, P2 types structures and so on in Figure S3) was set to less than 0.051 $Å^{-1}$.

Table S1. Refined atomic positions in $Na_{0.5}NbO_2$ at the room temperature in the hexagonal unit cell with a(=b)=2.94 Å and c=12.09 Å and the space-group P63/mmc.

	x	**y**	**z**	**occupancy**	**$B_{iso}(Å^2)$**
Na	0.0000	0.0000	0.0000	0.5	0.1
Nb	0.6609	0.3310	0.2567	1.0	0.1
O	0.3332	0.6667	0.1460	1.0	0.1

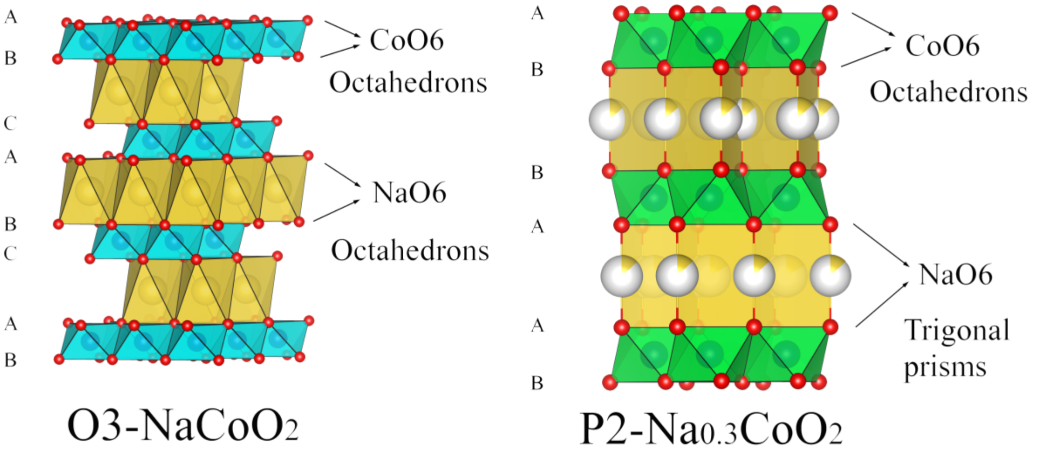

O3-$NaCoO_2$
(a)

P2-$Na_{0.3}CoO_2$
(b)

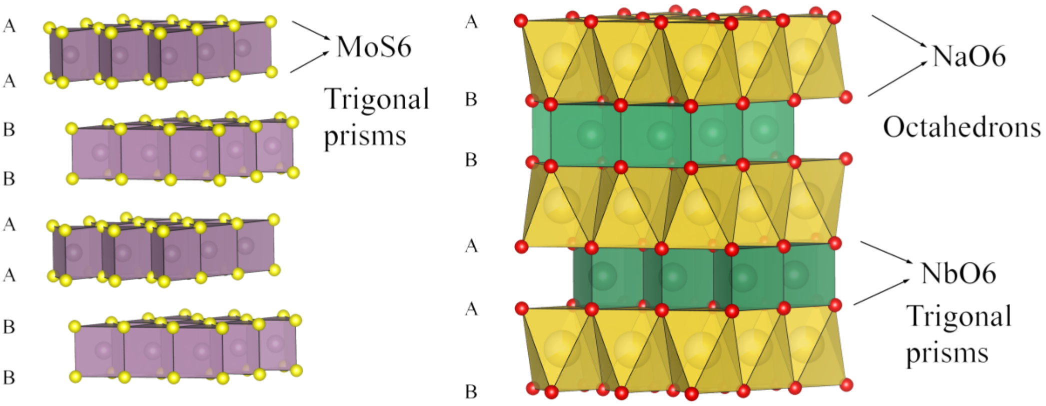

2H-MoS_2
(c)

anti-P2 $Na_{0.5}NbO_2$
(d)

Figure S1. Typical structural schematics of metal oxide/sulfide, examples as O3-$NaCoO_2$ (a), P2-$Na_{0.3}CoO_2$ (b), 2H-MoS_2 (c) and anti-P2 $Na_{0.5}NbO_2$ (d).

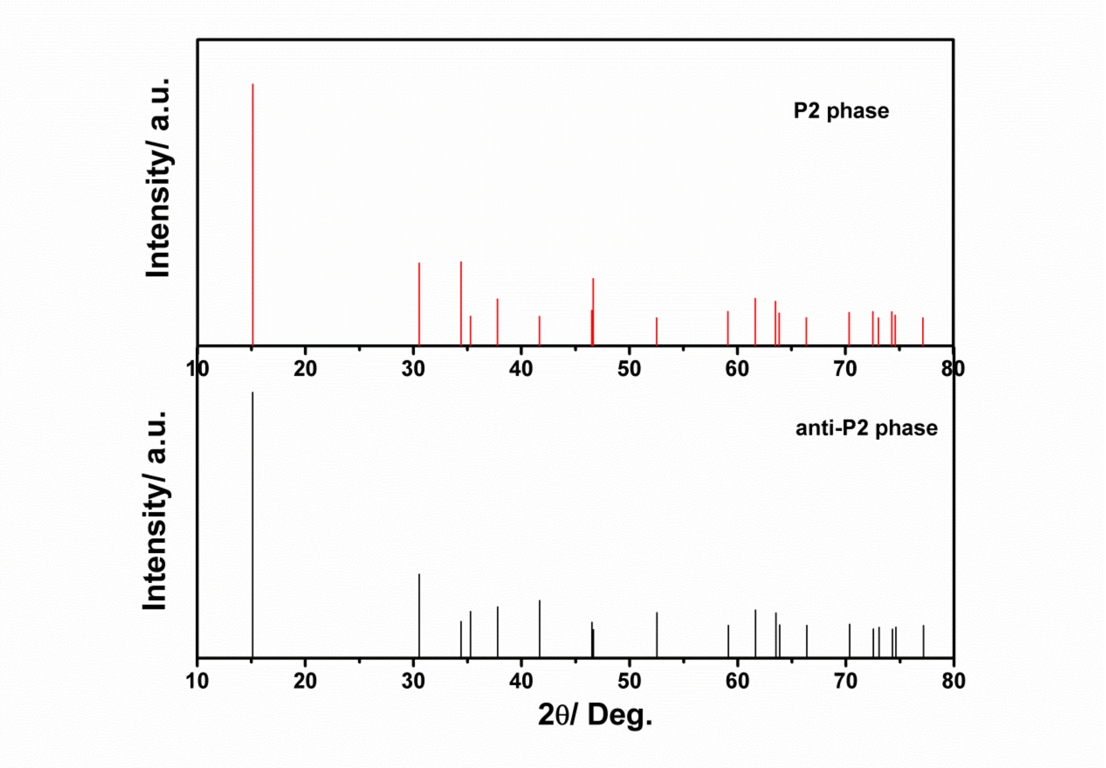

Figure S2. The fitting XRD patterns of anti-P2 and P2 type $NaNbO_2$ by Diamond program. The structures of these two phases share the same lattice parameters. The XRD patterns are of anti-P2 and P2 type phase are similar. Therefore, in fact, the anti-P2 and P2 type phases are indistinguishable from the XRD patterns when in consideration of other factors, such as particle size and orientation.

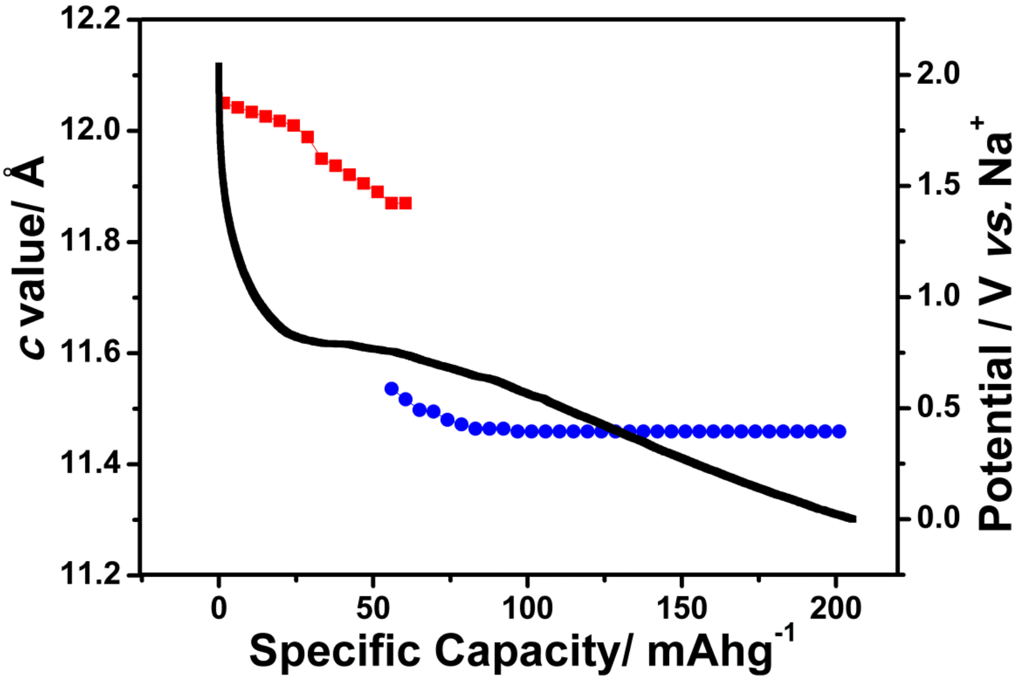

Figure S3. Changes of the lattice parameter *c* of Na_xNbO_2 during the first intercalation of Na ions.

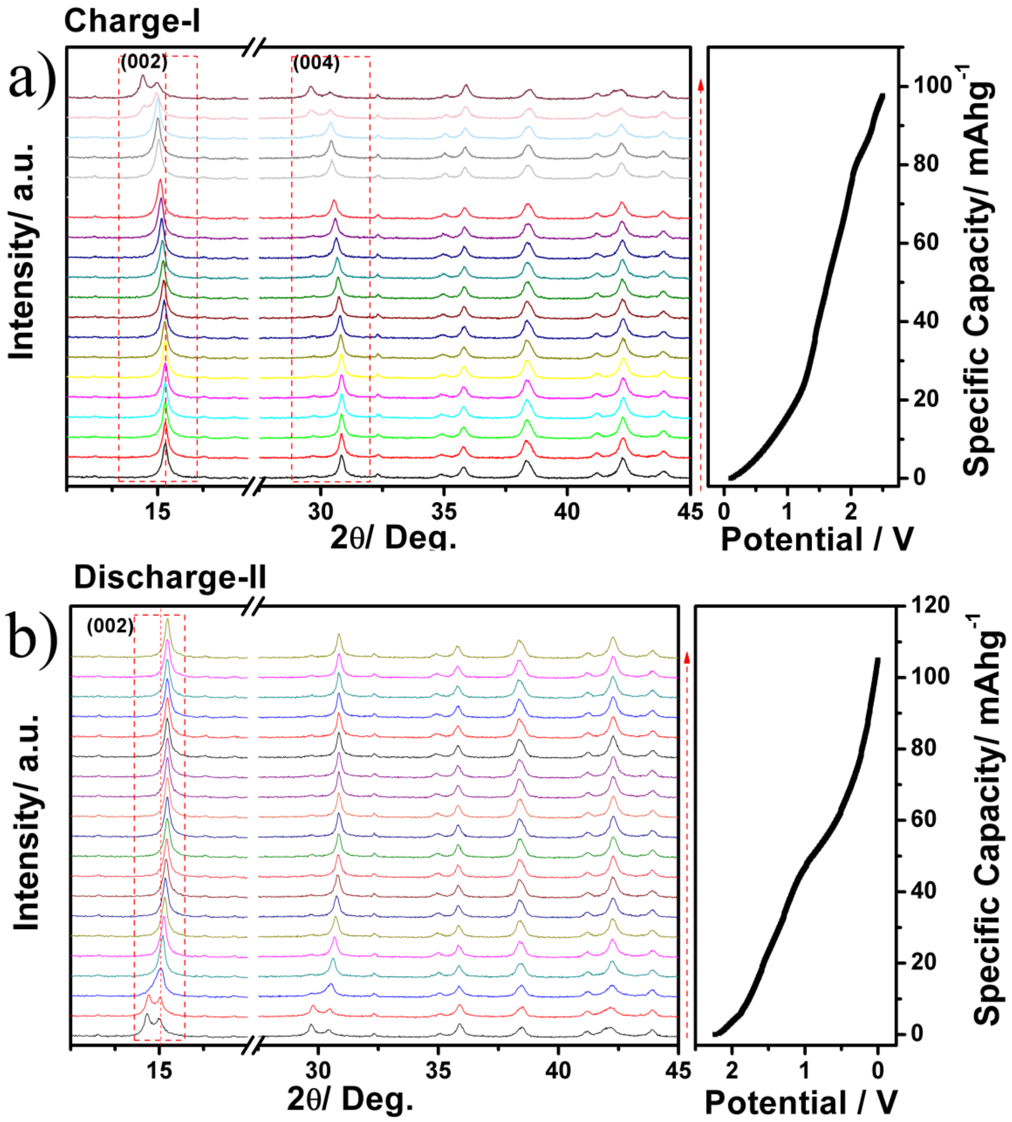

Figure S4. *In situ* XRD patterns of $Na_{0.5}NbO_2$ during electrochemical deintercalation (a) and reintercalation (b) of the Na ions.

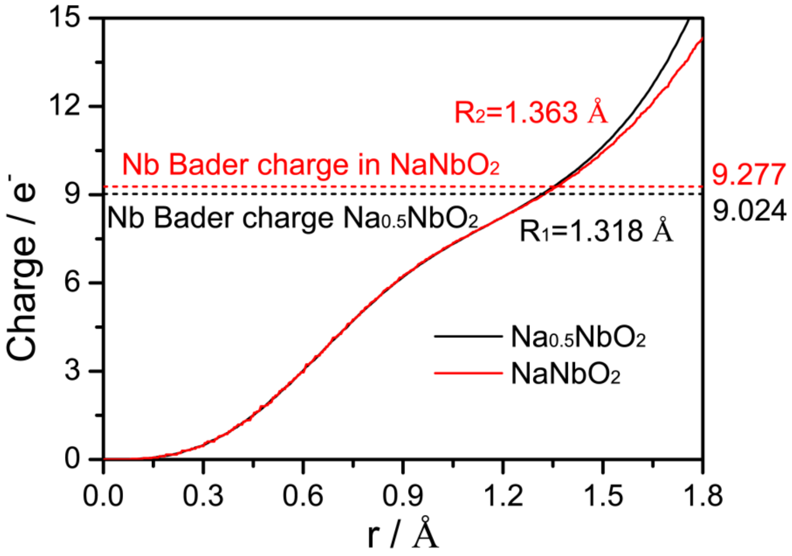

Figure S5. Amount of charge inside the Nb sphere.

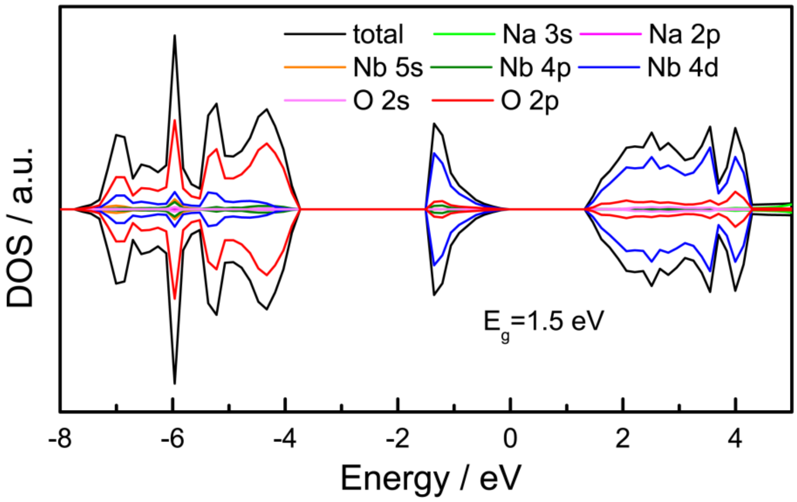

Figure S6. The DOS of $NaNbO_2$. The Fermi level is set to zero.

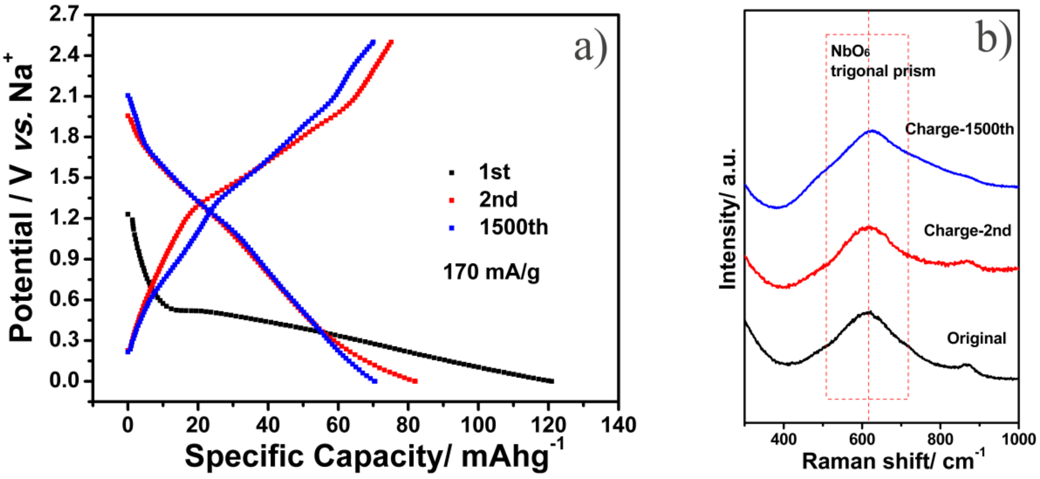

Figure S7. Potential profiles (a) and Raman spectra (b) of $Na_{0.5}NbO_2$ at the original, 2nd and 1500th charged states. The similarity of these Raman spectra demonstrates the high structural stability of $Na_{0.5}NbO_2$ with NbO6 trigonal prism.

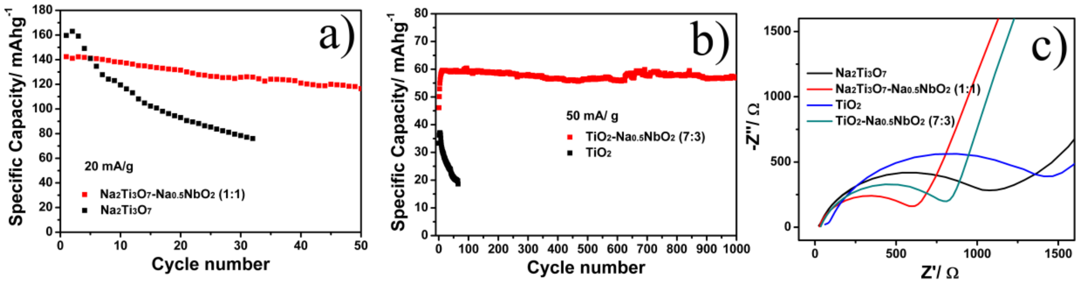

Figure S8. Cycling performances of $Na_2Ti_3O_7$-$Na_{0.5}NbO_2$ (1:1 wt%) (a) and TiO_2-$Na_{0.5}NbO_2$ (7:3 wt%) (b) and EIS of the composite with $Na_{0.5}NbO_2$ (c).

As shown in Figure S8a, the capacity retention of the $Na_2Ti_3O_7$-$Na_{0.5}NbO_2$ (1:1 wt%) composite is 81.8% after 50 cycles while that of pure $Na_2Ti_3O_7$ is only 47.6% after 32 cycles. In addition, long cycling life (1000 cycles) with stable reversible capacity of 58 mAh g^{-1} is achieved for the TiO_2-$Na_{0.5}NbO_2$ (7:3 wt%) composite (Figure S8b) at a high current density of 50 mA g^{-1} while pure TiO_2 exhibits negligible capacity with poor cycling life. It is worth noticing that these improvements are obtained by simply mixing $Na_{0.5}NbO_2$ with other active materials, further improvement can be achieved by homogeneously mixing or coating with $Na_{0.5}NbO_2$.

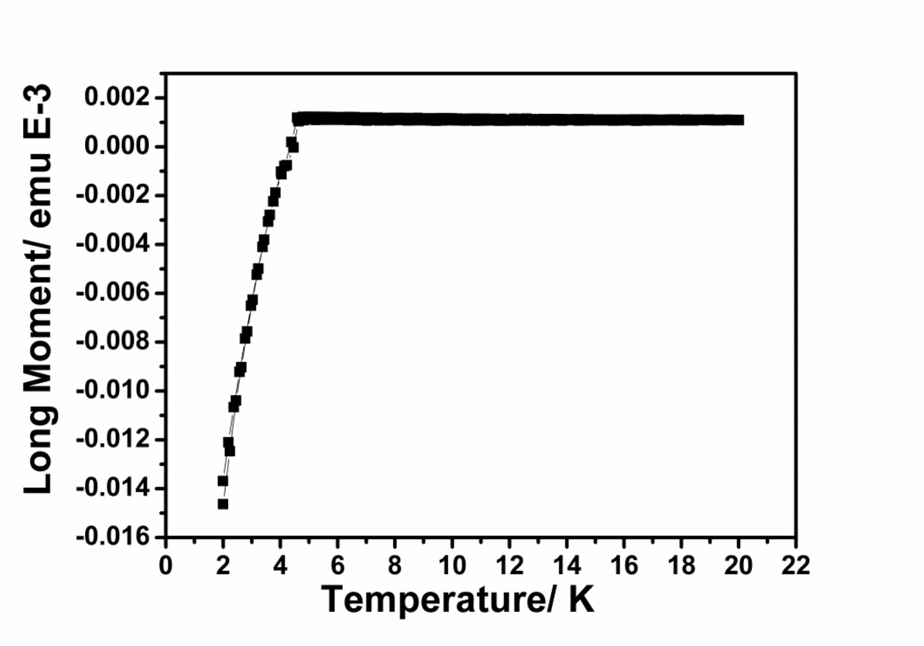

Figure S9. The changes of the magnetic susceptibility of the $Na_{0.5}NbO_2$ in the 2-20K temperature range. Its variance indicates that $Na_{0.5}NbO_2$ is a superconductor and the transition temperature is about 4.5K.

References

S1. Hohenberg P, Kohn W. Inhomogeneous Electron Gas. *Physical Review* **136**, B864-B871 (1964).

S2. Kohn W, Sham L. Self-Consistent Equations Including Exchange and Correlation Effects. *Physical Review* **140**, A1133-A1138 (1965).

S3. Kresse G, Furthmüller J. Efficient iterative schemes for ab initio total-energy calculations using a plane-wave basis set. *Phys Rev B* **54**, 11169 (1996).

S4. Blöchl PE. Projector augmented-wave method. *Phys Rev B* **50**, 17953 (1994).

S5. Perdew JP, Burke K, Ernzerhof M. Generalized gradient approximation made simple. *Phys Rev Lett* **77**, 3865 (1996).